Chinese Chemical Letters 32 (2021) 3393–3397

Contents lists available at ScienceDirect

Chinese Chemical Letters

journal homepage: www.elsevier.com/locate/cclet

Communication

A general strategy *via* photoelectrocatalytic oxygen reduction for generating singlet oxygen with carbon bridged carbon-nitride electrode

Qianqian Yang, Zhiyuan Feng, Mingyue Liu, Jinxing Zhang, Hongying Zhao*, Guohua Zhao

School of Chemical Science and Engineering, and Shanghai Key Lab of Chemical Assessment and Sustainability, Tongji University, Shanghai 200092, China

ARTICLE INFO

Article history:
Received 8 February 2021
Revised 20 April 2021
Accepted 27 May 2021
Available online 1 June 2021

Keywords:
Oxygen reduction reaction
Singlet oxygen
Photoelectrocatalytic process
Carbon-nitride
Wastewater treatment

ABSTRACT

With the ever-growing demand of clean water for the healthy world, water purification has become an urgent global issue. Singlet oxygen ($^1O_2$) as unique non-radical derivative of oxygen, possessing unoccupied π^* orbital and exhibiting high selectivity towards electron-rich organic pollutants. Nevertheless, most of the approaches suffer from low-efficiency or biotoxicity, which severely restrict their potential applications. Therefore, in this work, we propose a general strategy *via* photoelectrocatalytic for selectively reducing oxygen to $^1O_2$ with designed carbon bridged carbon nitride (CBCN). This work highlights the important role of synergistic photo-electro-catalytic effect for selectively generating the $^1O_2$ *via* oxygen reduction pathway, which can be a promising way especially for degrading electron-rich pollutants.

In recent decades, the overload discharge of refractory organics leads to water pollution, which would be threatened the sustainable development of society [1–3]. Meanwhile, the ever-growing demand on clean water has given rise to tremendous effort for developing environmentally friendly and efficient technologies for wastewater treatment. Singlet oxygen ($^1O_2$) is unique non-radical derivative of oxygen [4], possessing unoccupied π^* orbital and exhibiting high selectivity towards to electron-rich organic pollutants such as medicine [5,6] and pathogenic microorganism [7].

Greater recognition of the vital significance of $^1O_2$ has motivated research for more effective $^1O_2$ production [4]. In general, $^1O_2$ is produced *via* the energy transfer from a series of photosensitizers including organic dyes, fullerene derivates, porphyrins, and semiconductor quantum dots to the triplet ground state of O_2 [8]. Instead of the energy transfer, $^1O_2$ can be generated *via* the oxidation of $O_2^{\bullet-}$ through removing the electrons in the antibonding π^* orbitals of $O_2^{\bullet-}$ in electrocatalytic and/or photocatalytic process [4,9]. Nevertheless, most of the approaches suffer from such drawbacks as low quantum yield, poor selectivity, non-recyclability and biotoxicity, which severely restrict their potential applications.

Photoelectrocatalytic (PE) activation of O_2 has emerged as a promising and green alternative way to efficiently produce reactive oxygen species (ROS), because it can overcome the energy barrier with a high solar energy conversion efficiency [10]. In this process, O_2 is firstly reduced to $O_2^{\bullet-}$ through 1-electron reduction pathway, and then the generated $O_2^{\bullet-}$ would be simultaneously oxidized to $^1O_2$ by photoinduced hole (h_{vb}^+) [4,9,11]. The production efficiency of $^1O_2$ in PE system is mainly determined by the selectivity of oxygen reduction and the oxidation ability of h_{vb}^+. Graphitic carbon nitride (g-C_3N_4, denoted as CN) has attracted attention due to their special optical features and environmental friendliness [12–15]. It is a promising metal-free photocatalyst that can be widely used in environmental fields [16,17]. Nonetheless, the photocatalytic efficiency of pure CN was relatively low. Although transition metal doped CN with variable chemical states and unoccupied orbitals appear to be more efficient to improve photocatalytic performance [18,19], the problem of metallic ion leaching remains a significant concern for practical applications [1]. In contrast, doping non-metal elements, especially for self-doping of C atom, can not only expand the visible light absorption of CN, but also facilitate the charge transfer by forming delocalized π bonds [13,20,21]. However, most of the researches so far mainly focused on the direct oxidation of CN [21,22], few examples have paid attention to non-radical $^1O_2$ generated from CN. Besides, the photoelectrocatalytic mechanism on how to selectively generate $^1O_2$ by designing CN-derived electrodes remain elusive.

Herein, we turn our research interest to the rational design of CN-derived electrodes (CBCN), integrated with photocatalytic and electrocatalytic process, for selectively activating oxygen to $^1O_2$. The CBCN was modified by introducing delocalized π bonds and cyano group simultaneously into CN framework through thermal

* Corresponding author.
E-mail address: hyzhao@tongji.edu.cn (H. Zhao).

https://doi.org/10.1016/j.cclet.2021.05.066
1001-8417/

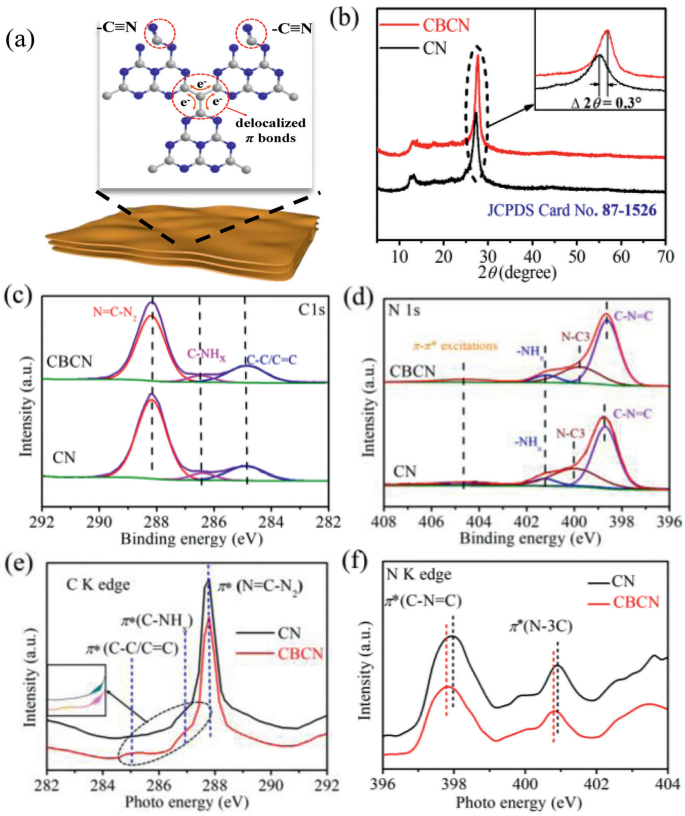

Fig. 1. Characterizations of catalysts. (a) Scheme illustration of CBCN. (b) XRD patterns of CBCN and CN. (c) XPS high-resolution C 1s spectra and (d) N 1s spectra. (e) Carbon K edge and (f) Nitrogen K edge XANES spectra of CBCN and CN.

polymerization method. As expected, the CBCN/PE system exhibits 100% removal efficiency for electron-rich pollutants such as bisphenol A (BPA) and acetaminophen (ACT). Moreover, CBCN/PE system with reliability and wide pH range toward the degradation process exhibits great practical application prospects in wastewater treatment field.

As we known, creating large delocalized π bonds in the framework of CN and introducing cyano group could improve the photocatalytic ability of pure CN [13,23,24]. An environmental begin and facile strategy of adjusting polymerization of CN precursors was proposed to fabricate carbon bridged carbon nitride (CBCN) containing π bonds and cyano functional group. As expected, the delocalized π bonds in CBCN was formed by substituting bridge N atom with C atom, and the cyano groups originated from the incomplete condensation of dicyandiamide (Fig. 1a). The crystalline structure of CN and CBCN were probed by X-ray diffraction (XRD). Both CN and CBCN have two peaks at 27.5° and 13.0° (Fig. 1b), corresponding to the interlayer stacking (002) and in-plane ordering of heptazine units (100) [25,26]. The layer stacking peak of CBCN was positively shifted 0.3° due to the increased stacking density of conjugated layers [13]. Besides, CBCN exhibited typical layered structure of g-C_3N_4 with more pores on its surface, possibly due to formation of NH_3 and CO_2 during the incomplete thermal decomposition of ammonium citrate (Fig. S1 in Supporting information) [21]. The specific surface area of CBCN was 15 m^2/g, larger than that of CN (8 m^2/g). Adsorption isotherms (Fig. S2 in Supporting information) and pore size distribution (Fig. S3 in Supporting information) indicated that CN and CBCN mainly contained mesopores. The pore volume of CBCN (0.090 cm^3/g) compared to CN (0.047 cm^3/g) also demonstrated the enhanced porosity of CBCN. Typical Fourier transform infrared (FTIR) bands of cyano groups (−C≡N) centered at 2177 cm^{-1} was only obtained for CBCN (Fig. S4 in Supporting information) [24]. Further information about the structure of the catalysts was explored by X-ray photoelectron spectroscopy (XPS) and X-ray absorption near edge structure (XANES) measurements. As exhibited in Fig. 1c, the C 1s spectrum can be deconvolved into three peaks with binding energies of 288.1 eV, 286.4 eV and 284.9 eV ascribed to C1 (N=C−N_2 in the framework of CN), C2 (C−NH_x on the edges of heptazine units) and C3 (C−C/C=C) [27,28]. The peak area ratio for C3 and C1 was calculated to be 0.19 and 0.35 for CN and CBCN, respectively. Moreover, XPS N 1s spectrum of CBCN was separated into four peaks with binding energies of 398.6 eV, 399.6 eV, 401.1 eV and 404.6 eV ascribed to N1 in the heptazine units (sp^2 structure of C−N=C), N2 (sp^3 bridging N of N−C3), N3 (−NH_x) and N4 (π-π^* excitations) (Fig. 1d) [24]. The peak area ratios of N2 and N1 was 0.54 and 0.42 respectively for CN and CBCN. These conclusions confirmed the replacement of bridging N with C after carbon doped [13,20]. In addition, comparing to CN, N1, N2 peaks of CBCN shift to lower binding energy, which due to the existence cyano groups whose N 1s binding energy are intermediate between those of N1 and N2 [21,23,24]. These observations were further verified by the normalized N 1s and C 1s K edge XANES spectra. As revealed in Fig. 1e, a decrease of N=C−N_2 as well as an increase of C−C/C=C and C−NH_x from CN to CBCN was observed, which was consistent with the C 1s XPS results. Besides, as shown in Fig. 1f, the C−N=C and N−C3 peaks of CBCN slightly shift to lower a binding energy and N-C3 showed weaker peak than CN.

The valence band maximum (VBM) and conduction band minimum (CBM) of CN and CBCN could be calculated from bandgap energies and Mott–Schottky curves (Fig. S5 in Supporting information). As shown in Fig. 2a, the conduction band potential of CBCN (−0.3 V *vs.* SHE) suggested the photogenerated electron (e_{cb}^-) could reduce O_2 to produce $O_2^{\bullet-}$ (−0.16 V *vs.* SHE) [29]. Moreover, CBCN exhibited 0.45 V positive valence band potential than CN, indicating the stronger oxidation ability of photogenerated hole (h_{vb}^+) that can oxidize $O_2^{\bullet-}$ to produce $^1O_2$. In order to verify the catalytic mechanism for selectively generating $^1O_2$ through photoelectrochemical reduction of O_2, electron paramagnetic resonance (EPR) measurement was carried out for investigating the formation of active oxygen species (ROS) such as $^{\bullet}OH$, $O_2^{\bullet-}$ and $^1O_2$. Obviously, as shown in Fig. 2b, the main ROS with CBCN in photoelectrocatalytic (PE) process was $^1O_2$. The EPR intensity of DMPO-$^{\bullet}OH$ was relatively weak compared to TEMP-$^1O_2$. Almost no $O_2^{\bullet-}$ species were detected in PE process both for CBCN and CN, possibly due to that $O_2^{\bullet-}$ was simultaneously transferred to $^1O_2$ [30]. Besides, the EPR intensity of TEMP-$^1O_2$ with CBCN was much stronger than CN, indicating the enhanced oxidation ability of h_{vb}^+ by the substitution of N atoms with bridged C atoms and cyano group. The synergistic effect of photocatalytic- and electrocatalytic-reduction of oxygen was summarized in Figs. 2c and d. Interesting, the EPR intensity of TEMP-$^1O_2$ in PE was almost 6–9 times higher than in sole electrocatalytic (E) and photocatalytic process (P) with CBCN. In PE system, O_2 was firstly reduced to $O_2^{\bullet-}$ by electrons (e^-) from external circuit in E system and/or e_{cb}^- in P system through single electron pathway, and then h_{vb}^+ oxidized $O_2^{\bullet-}$ to form $^1O_2$ (Eq. 1) [4,9]. That is why the formation of $^1O_2$ is more efficient in PE system. To further confirm the generation pathway of $^1O_2$ in PE process, the ethylenediaminetetraacetic acid disodium salt (EDTA-2Na) and potassium dichromate ($K_2Cr_2O_7$) were respectively used as scavengers of h_{vb}^+ and e_{cb}^- (Fig. 2c). The intensity of TEMP-$^1O_2$ with CBCN almost remained the same after the addition of $K_2Cr_2O_7$, indicating that e_{cb}^- had little effect in the formation of $^1O_2$. That is to say, the formation of $O_2^{\bullet-}$ in PE process was mainly contributed by e^- from external circuit in E system. However, the $^1O_2$ was obviously inhibited once using EDTA-2Na to capture h_{vb}^+. Note that, comparing to CBCN, h_{vb}^+ had a less im-

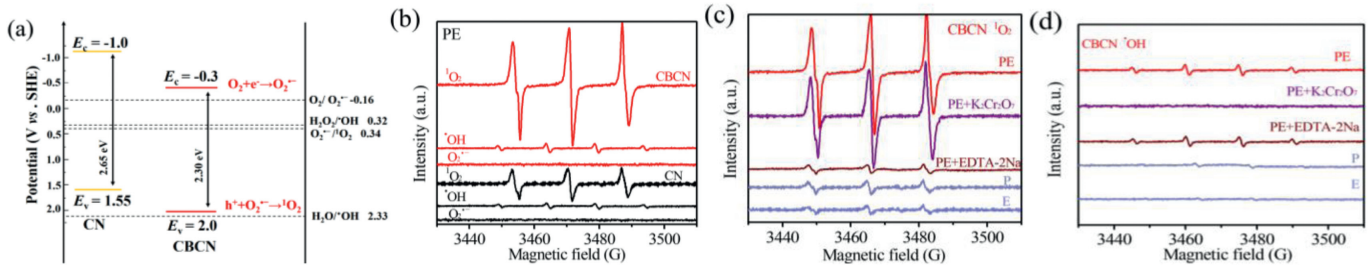

Fig. 2. (a) Band structure alignments for CBCN and CN. (b) EPR spectra of $^1O_2$, •OH and O_2•⁻ in PE process. (c) CBCN EPR spectra of $^1O_2$ in different processes (PE, P, and E represent photoelectrocatalytic, photocatalytic and electrocatalytic process). The EDTA-2Na and $K_2Cr_2O_7$ were quenching agent for h_{vb}^+ and e_{cb}^-, respectively. (d) CBCN EPR spectra of •OH under different reaction conditions.

pact on the generation of $^1O_2$ for CN (Fig. S7 in Supporting information). This observation indicated that the delocalized π bonds and cyano groups in CBCN greatly favor the formation of $^1O_2$. In the sole E process, the generation of $^1O_2$ was originated from the oxidation of O_2•⁻ with surface •OH (•OH_{sur}), which acted as surface trapped holes (Eq. 2) [9]. The low generation efficiency of •OH in E system resulted in the weak intensity of TEMP-$^1O_2$.

$$O_2 \xrightarrow{e^-/e_{cb}^-} O_2^{\bullet -} \xrightarrow{h_{vb}^+} {}^1O_2 \quad (1)$$

$$O_2 \xrightarrow{e^-} O_2^{\bullet -} \xrightarrow{{}^{\bullet}OH_{sur}} {}^1O_2 \quad (2)$$

The intensity of generated •OH in PE process was relatively stronger than in sole E and P systems for CBCN. The intensity of DMPO-•OH was almost vanished in the presence of $K_2Cr_2O_7$ in PE system, while remained the same with the addition of EDTA-2Na as the scavenger of h_{vb}^+. This phenomenon indicated that e_{cb}^- was active sites for reducing electrochemical generated H_2O_2 to generate •OH radicals in PE process. In fact, H_2O_2 was formed *via* 2-electron reduction pathway of oxygen reduction reaction (ORR). In P system, the adsorbed O_2 on the surface of the catalyst was reduced by e_{cb}^- to generate O_2•⁻, then, O_2•⁻ react with H^+ and e_{cb}^- to generate •OH (Eq. 3) [9]. Different with PE and P systems, in E process, almost no •OH was obtained, confirming that there are no active sites in CBCN for decomposing H_2O_2.

$$O_2 \xrightarrow{e_{cb}^-} O_2^{\bullet -} \xrightarrow{e_{cb}^-} {}^{\bullet}OH \quad (3)$$

The delocalized π bonds and cyano group can change the electronic structure and modify the band gap of CN, thus increasing the light absorption ability and charge separation efficiency. As shown in Fig. 3a, CBCN would adsorb more visible light than CN to generate more photogenerated electron-hole pairs. In addition, 70 nm redshift in the adsorption edge was obtained for CBCN. According to the Tauc plots, as shown in Fig. 3b, the band gaps of CBCN and CN can be obtained by the linear extrapolation of a straight line with the baseline [23]. The band gaps of CBCN and CN were determined to be 2.30 and 2.65 eV, respectively. The charge separation efficiency was further clarified by photoluminescence (PL) spectra measurements. As shown in Fig. 3c, the PL intensity of CBCN was much lower than CN, indicating the improved separation of photoexcited charge carriers [31]. The observation indicated that cyano groups can introduce intraband states into the band gap of CN and carbon species in bridged carbon can act as electron sink, inhibiting the recombination of photogenerated electron-hole pairs [21].

The internal electron transport capability was characterized by electrochemical impedance spectroscopy. Fig. 3d presented that the Nyquist plots diameter of CBCN was much smaller than that of CN, indicating that the conductivity and internal electron transmission capacity were enhanced due to the formation of delocalized big π bonds [13]. Fig. 3e demonstrated that the photocurrent response of CBCN was 3 times higher than CN under the same conditions, suggesting the fabricated CBCN with delocalized π bonds and cyano group exhibited excellent photocatalysis performance and can be a promising electrophotocatalyst for wastewater treatment. The selectivity and activity of oxygen reduction reaction were investigated by rotating ring-disk electrode (RRDE) measurement. The linear sweep voltammetry (LSV) results suggested that the improved ORR activity was obtained for CBCN with 300 mV positive shift of the onset potential, but decreased the 2e⁻ ORR selectivity with a declined ring current (Fig. 3f). The H_2O_2 selectivity (%H_2O_2) for CBCN and CN at −0.21 V (*vs.* SHE) were respectively 55% and 66%. The slight decrease in %H_2O_2 *via* 2e⁻ ORR with CBCN was possibly due to the decreased concentration of pyrrolic-N during the substation of C atom for bridge N in CN [32].

As investigated above, the selective formation of $^1O_2$ *via* photoelectrocatalytic oxygen reduction can be successfully achieved with CBCN in this work. Moreover, $^1O_2$ is a more selective oxidant (1.1 V *vs.* SHE) than •OH, which can preferentially oxidize electron-rich organic pollutants [33]. Therefore, we further evaluated the role of $^1O_2$ by estimating the degradation efficiency of BPA, ACT and 3-chlorophenol (3-CP) with different charge density. According to Fig. 4a, the apparent rate constants (k_{obs}) of removing BPA, ACT and 3-CP could be fitted with pseudo-first-order kinetic model. And the value of k_{obs} for BPA was 0.140 min^{-1}, which is 7.8 and 2.2 times higher than 3-CP (0.018 min^{-1}) and ACT (0.063 min^{-1}), respectively. Compared to the organics with electron-donating groups such as BPA, ACT and 3-CP, the degradation rate of nitrobenzene (NB) without electron-donating was obviously lower (0.0057 min^{-1}) (Fig. S9 in Supporting information). The generated $^1O_2$ in CBCN/PE system has strong electrophilic ability, so BPA with highest charge density exhibited significant degradation, moderate and lowest degradation was respectively obtained for ACT and 3-CP. To identify the role of different active spices ($^1O_2$, •OH, h_{vb}^+) on the removal of BPA, ACT and 3-CP, quenching experiments were designed. L-histidine and isopropanol (IPA) were used as scavengers to capture $^1O_2$ and •OH respectively. As exhibited in Fig. 4b, the degradation efficiency of BPA was decreased from 100% to 90.5% and 9.4% after the addition of IPA and L-histidine, respectively. The addition of IPA and L-histidine resulted the ACT removal efficiency decreased to 68.1% and 29.7%. Note that, the degradation efficiency of 3-CP was greatly decreased to 15.5% in the presence of IPA. Besides, the degradation of efficiency of BPA, ACT and 3-CP was respectively decreased to 17.2%, 38.5% and 70.8% after the addition of EDTA-2Na as h_{vb}^+ scavenger. This phenomenon reveals that $^1O_2$ and h_{vb}^+ played significant role

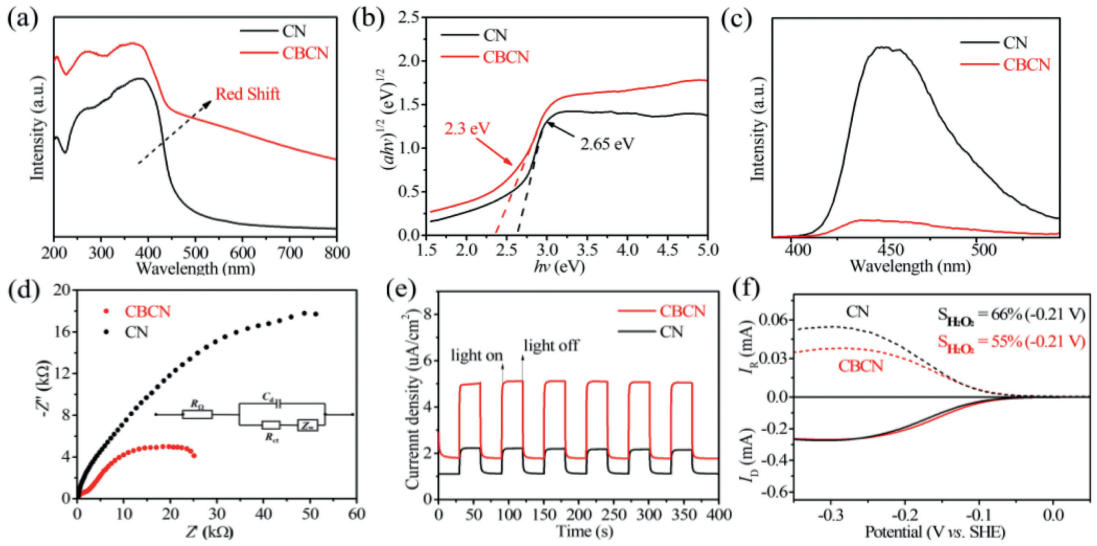

Fig. 3. (a) UV–vis DRS and (b) band gap energy and (c) the steady-state photoluminescence spectra (PL) of CN and CBCN. (d) Electrochemical impedance spectroscopy. (e) Transient photocurrent responses of photo catalysts in 0.05 mol/L Na_2SO_4 aqueous solution under visible light irradiation. (f) LSV curves of CBCN and CN recorded at 1600 rpm and at a rate of 10.0 mV/s, demonstrating the ORR current density on the disk (I_D) and the detected H_2O_2 currents on the ring electrode (I_R).

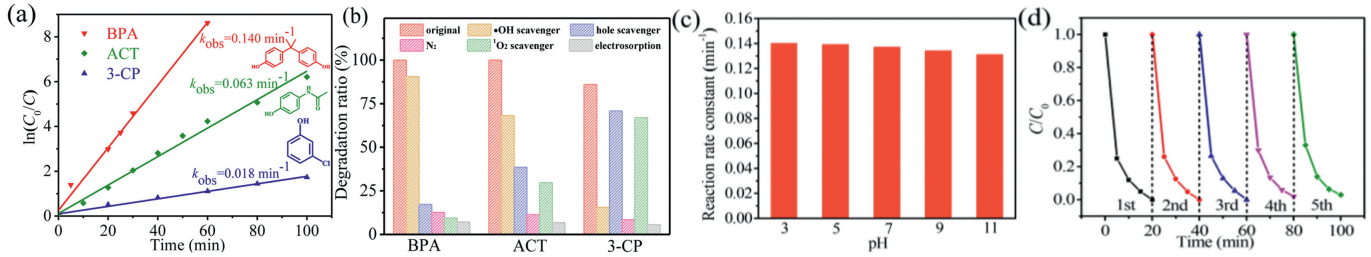

Fig. 4. (a) Kinetic curves in the degradation process of BPA, ACT and 3-CP by CBCN/PE at pH 3. The initial concentration of all pollutants was 10 ppm. (b) The quenching experiment of BPA, ACT and 3-CP on PE degradation under different conditions ($[BPA]_0 = [ACT]_0 = [3\text{-}CP]_0$ = 10 mg/L, [IPA] = [EDTA-2Na] = [L-histidine] = 2 mmol/L). (c) The effect of pH value on BPA degradation efficiency in PE process. (d) The stability of CBCN/PE in the BPA degradation process.

for BPA and ACT removal, while •OH was relatively responsible for 3-CP removal. In addition, the PE degradation process under N_2 atmosphere was carried out to exclude the oxidation contribution of ROS. As shown in Fig. 4b, the degradation efficiency of BPA, 3-CP, ACT was only 12.6%, 11.3% and 8.4%. In order to further clarify the contribution of h_{vb}^+, the electrosorption of BPA (7.1%), ACT (6.7%) and 3-CP (5.6%) with electrode was investigated. All the observation revealed that the contribution of h_{vb}^+ on the degradation of organic pollutants can be ignored. The role of h_{vb}^+ was acted for the generation of $^1O_2$.

As we known, actual wastewater had variable pH values, and thus, it is necessary to determine the effect of pH values on the degradation efficiencies. As shown in Fig. 4c, obviously, the BPA removal rate constant remained as high as 0.14–0.13 min^{-1} in the wide pH range of 3–11. This phenomenon was attributed that h_{vb}^+ was active sites for oxidizing electro/photochemical generated $O_2^{\bullet-}$ to produce $^1O_2$ for BPA removal. The generation route of $^1O_2$ was not restricted by pH value. As shown in Fig. 4d, the degradation efficiency of BPA was nearly maintained at the level of fresh sample after five consecutive runs, indicating that this fabricated CBCN cathode exhibited good stability. Based on above results, the CBCN/PE system exhibited great practical application prospects in wastewater treatment field.

In summary, we have constructed a metal free CBCN/PE system for selective generation of $^1O_2$ *via* oxygen reduction, and then applied for efficient degradation of electron-rich organic pollutants. The CBCN was modified by introducing delocalized π bonds and cyano group simultaneously into CN framework through thermal polymerization method. The delocalized π bonds and cyano group in CBCN change the electronic structure of CN for both enhancing the photocatalytic and electrocatalytic activity. In CBCN/PE system, O_2 was firstly reduced to $O_2^{\bullet-}$ *via* 1-electron pathway, and then the produced $O_2^{\bullet-}$ would be simultaneously oxidized by h_{vb}^+. As expected, the CBCN/PE system exhibits 100% removal efficiency for electron-rich pollutants such as bisphenol A (BPA) and acetaminophen (ACT). This study supplies a general strategy for the spontaneous formation of abundant $^1O_2$ *via* PE oxygen activation. Hence, we expect this green, simple and economic strategy to prepare nonmetal CBCN/PE system with excellent capability could have broad application in water treatment filed.

Declaration of competing interest

The authors declare that they have no known competing financial interests or personal relationships that could have appeared to influence the work reported in this paper.

Acknowledgments

The authors acknowledge funding from the National Natural Science Foundation of China (Nos. 22076142, 21677106, 22076140), National Key Basic Research Program of China (No. 2017YFA0403402), National Natural Science Foundation of China (No. U1932119), the Science & Technology Commission of Shanghai Municipality (No. 14DZ2261100), the Fundamental Research Funds for the Central Universities.

Supplementary Materials

Supplementary material associated with this article can be found, in the online version, at 10.1016/j.cclet.2021.05.066.

References

[1] Y. Gao, Z. Chen, Y. Zhu, T. Li, C. Hu, Environ. Sci. Technol. 54 (2020) 1232–1241.
[2] H. Wang, J. Zhang, P. Wang, et al., Chin. Chem. Lett. 31 (2020) 2789–2794.
[3] S. Liu, M. Zhao, Z. He, et al., Chin. J. Catal. 40 (2019) 446–457.
[4] Y. Zhao, M. Sun, X. Wang, et al., Nat. Commun. 11 (2020) 6228.
[5] J.A. Rengifo-Herrera, K. Pierzchała, A. Sienkiewicz, et al., Appl. Catal. B: Environ. 88 (2009) 398–406.
[6] S.Y. Dong, Y.L. Zhao, J.Y. Yang, et al., Appl. Catal. B: Environ. 291 (2021) 120127.
[7] D. García-Fresnadillo, ChemPhotoChem. 2 (2018) 512–534.
[8] F. Yang, X. Chu, J. Sun, et al., Chin. Chem. Lett. 31 (2020) 2784–2788.
[9] Y. Nosaka, A.Y. Nosaka, Chem. Rev. 117 (2017) 11302–11336.
[10] D. Pan, S. Xiao, X. Chen, et al., Environ. Sci. Technol. 53 (2019) 3697–3706.
[11] S. Zhao, X. Zhao, Appl. Catal. B: Environ. 250 (2019) 408–418.
[12] H. Zhan, Y. Wang, X. Mi, et al., Chin. Chem. Lett. 31 (2020) 2843–2848.
[13] G.H. Dong, K. Zhao, L.Z. Zhang, Chem. Commun. 48 (2012) 6178–6180.
[14] Q. Hao, C.a. Xie, Y. Huang, et al., Chin. J. Catal. 41 (2020) 249–258.
[15] J. Xiong, X.B. Li, J.T. Huang, et al., Appl. Catal. B: Environ. 266 (2020) 118602.
[16] X. Wang, K. Maeda, A. Thomas, et al., Nat. Mater. 8 (2009) 76–80.
[17] D. Chen, K. Wang, W. Hong, et al., Appl. Catal. B: Environ. 166-167 (2015) 366–373.
[18] D. Chen, K. Wang, D. Xiang, et al., Appl. Catal. B: Environ. 147 (2014) 554–561.
[19] S.Y. Dong, L.F. Cui, Y.J. Tian, et al., J. Hazard. Mater. 399 (2020) 123017.
[20] H. Li, F. Li, Z. Wang, et al., Appl. Catal. B: Environ. 229 (2018) 114–120.
[21] Z.H. Li, D.L. Huang, C.Y. Zhou, et al., Chem. Eng. J. 382 (2020) 122657.
[22] Q. Zheng, E. Xu, E. Park, H. Chen, D. Shuai, Appl. Catal. B: Environ. 240 (2019) 262–269.
[23] S. Wu, H. Yu, S. Chen, X. Quan, ACS. Catal. 10 (2020) 14380–14389.
[24] H. Yu, R. Shi, Y. Zhao, et al., Adv. Mater. 29 (2017) 1605148.
[25] Q. Liu, D. Zhu, M. Guo, Y. Yu, Y. Cao, Chin. Chem. Lett. 30 (2019) 1639–1642.
[26] M. Liu, D. Zhang, J. Han, et al., Chem. Eng. J. 382 (2020) 123017.
[27] M. Mohamed, M. Zain, L. Minggu, et al., Appl. Catal. B: Environ. 236 (2018) 265–279.
[28] X.B. Li, B.B. Kang, F. Dong, et al., Nano Energy 81 (2021) 105671.
[29] Q. Zheng, D. Durkin, J. Elenewski, et al., Environ. Sci. Technol. 50 (2016) 12938–12948.
[30] Z. Yang, J. Qian, A. Yu, B. Pan, Proc. Natl. Acad. Sci. U. S. A. 116 (2019) 6659–6664.
[31] J. Hu, P. Zhang, W. An, et al., Appl. Catal. B: Environ. 245 (2019) 130–142.
[32] L.Q. Li, C. Tang, Y. Zheng, et al., Adv. Energy Mater. 10 (2020) 2000789.
[33] J. Brame, M. Long, Q. Li, P. Alvarez, Water. Res. 60 (2014) 259–266.